Bulletin of the Seismological Society of America, Vol. 99, No. 2A, pp. 694–704, April 2009, doi: 10.1785/0120070211

Combination of Acceleration-Sensor and Broadband Velocity-Sensor Recordings for Attenuation Studies: The Case of the 8 January 2006 Kythera Intermediate-Depth Earthquake

by A. A. Skarlatoudis, C. B. Papazachos, B. N. Margaris, Ch. Papaioannou, Ch. Ventouzi, D. Vamvakaris, A. Bruestle, T. Meier, W. Friederich, G. Stavrakakis, T. Taymaz, R. Kind, A. Vafidis, T. Dahm, and EGELADOS Group

Abstract On 8 January 2006, an intermediate-depth earthquake occurred at the western part of the Hellenic trench close to the island of Kythera (southern Greece). This is the first intermediate-depth earthquake in the broader Aegean area that has produced such an extensive set of useful recordings, as it was recorded by the main permanent seismological networks and numerous acceleration sensors operating in Greece, as well as by EGELADOS, a large-scale temporary amphibian broadband seismological network deployed in the southern Aegean area.

An effort to combine all the available data (broadband velocity and acceleration sensor) was made to study the properties of ground-motion attenuation of this earthquake. The combination of both types of data revealed interesting properties of the earthquake wave field, which would remain hidden if only one type of data was used. Moreover, the data have been used for a validation of existing peak ground-motion empirical prediction relations and the preliminary study of the very inhomogeneous attenuation pattern of the southern Aegean intermediate-depth events at both near- and far-source distances.

Introduction

The Kythera intermediate-depth earthquake (**M** 6.7, depth = 67 km) occurred in the western part of the Hellenic arc (Fig. 1). Most of the damage was observed in the village Mitata of Kythera Island (Karakostas *et al.*, 2006). The earthquake was strongly felt in all regions of Greece and in a very large area of the eastern Mediterranean Sea, from southern Italy to Egypt and Jordan. Figure 1 shows the epicenters and focal mechanisms computed by several institutes for the 2006 Kythera earthquake. The inversion of broadband and teleseismic waveforms revealed a reverse focal mechanism with a strike-slip component (strike, 50; dip, 55; rake, 115) (Benetatos and Kiratzi, 2006), in accordance with the regional stress field for the western Hellenic arc at this depth range (in-slab intermediate-depth events), where northwest–southeast compression following the local trend of the Hellenic arc and northeast–southwest down-dip extension, parallel to the dip of the subducting slab are observed (Kiratzi and Papazachos, 1995). In Figure 1 the typical (average) focal mechanisms (light gray) computed by Papazachos *et al.* (2000) using all the available intermediate-depth focal mechanisms for different segments of the Benioff zone of the Hellenic arc are also shown. The striking similarity between the expected focal mechanism for intermediate-depth events in the broader Kythera Island area (mechanism d2) and the proposed focal mechanism for the 2006 Kythera earthquake verifies the agreement of the Kythera event faulting with regional tectonics.

Several empirical predictive studies have been performed for subduction zones worldwide, including Greece, with the use of strong-motion data (Theodulidis and Papazachos, 1990; Crouse, 1991; Youngs *et al.*, 1997). Atkinson and Boore (2003) were among the first ones that combined velocity-sensor and acceleration-sensor data from different subduction zones to derive empirical ground-motion relations for deep events of Cascadia and other regions. The use of both data types has certain advantages, such as overcoming the near-source clipping of broadband velocity-sensor recordings by the use of acceleration-sensor recordings. On the other hand, broadband velocity-sensor recordings can balance the lack of observations and/or the artificial trigger-level clipping, introduced at large distances by acceleration-sensors, resulting in a significant bias of acceleration-sensor prediction relations (e.g., Fukushima, 1997).

In the present article a detailed study of the inhomogeneous attenuation pattern of the Kythera intermediate-depth event is examined, comparing back-arc and along-arc at-

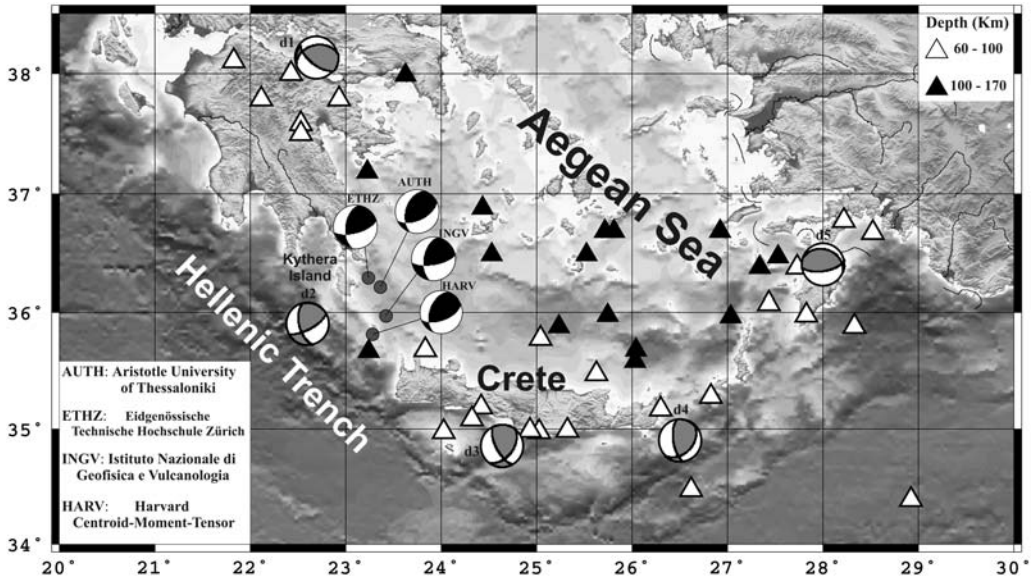

Figure 1. Map of the epicenters and focal mechanisms determined for the 2006 Kythera intermediate-depth earthquake (black compressive parts) and average focal mechanisms for different Benioff zone segments along the Hellenic arc (light gray compressive parts) (after Papazachos *et al.*, 2000). Historical intermediate-depth earthquakes (Papazachos and Comninakis, 1971) are also shown in this map defining the shape of the Benniof zone, with black (depth 100–170 km) and white (depth 60–100 km) triangles.

tenuation patterns. Moreover an evaluation of the applicability of different empirical prediction relations in the observed data is performed and preliminary empirical prediction relations for peak ground acceleration (PGA) and peak ground velocity (PGV) are derived.

Data Used

The 2006 Kythera intermediate-depth earthquake was recorded by the permanent seismological networks in the Aegean area among which are the two main permanent seismological Greek networks, operated by the National Observatory of Athens and the Aristotle University of Thessaloniki. However, the main body of broadband velocity-sensor recordings for this earthquake came from EGELADOS, a large-scale temporary amphibian broadband seismological network deployed in the southern Aegean area, coordinated by the Ruhr-University of Bochum (Germany) and operated by a large working group involving the Aristotle University of Thessaloniki (Greece), the National Observatory of Athens, Technical University of Chania, Istanbul Technical University (Turkey), University of Hamburg, and GeoForschungszentrum Potsdam (Germany). Despite the amphibian character of the EGELADOS network, only data from the land stations were used, because the OBS stations were not yet installed when the Kythera event occurred. Additional broadband velocity-sensor recordings from the National Observatory of Athens, Kandilli Observatory and Earthquake Research Institute (KOERI), and GEOFON permanent stations were also included in the broadband velocity-sensor data set.

The corresponding acceleration-sensor data set was compiled using all the available data recorded by the acceleration-sensor networks operated by the Institute of Engineering Seismology and Earthquake Engineering (ITSAK), the Geodynamic Institute of the National Observatory of Athens (Konstantinou *et al.*, 2006), the Public Power Corporation (PPC), and the Astronomical Observatory of Larissa. In Figure 2 broadband velocity-sensor stations where recordings were available are shown with triangles, while acceleration-sensor stations are denoted with squares. For data availability, see the Data and Resources section.

Instrument Information

The majority of velocity sensors used were broadband (typically 60 sec–50 Hz). Velocity-sensor recordings derived from short-period sensors were excluded from the data set, because intermediate-depth earthquakes are rich in their low-frequency content and short-period recordings may not properly represent these features. Most of the broadband sensors used were different types of Guralp sensors (mainly CMG-3ESP) and Streckeisen STS-2, while the data loggers employed were mostly of 24 and 18 bit (in some cases) resolution. On the other hand, most of the acceleration-sensor instruments had low-resolution digitizers (11 bit, Kinemetrics QDR with micro electro mechanical systems technology) and only a small number of them were of higher resolution (18 bit [Geosig GSR18 and Kinemetrics ETNA] and 24 bit [GURALP CMG-5T]). More information about the instrumentation and data logging can be found in the corresponding Web sites of the contributing institutes.

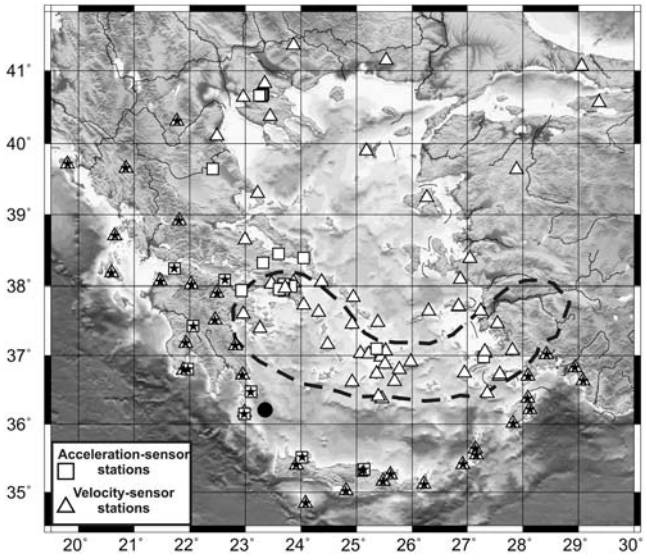

Figure 2. Network coverage of the 2006 Kythera intermediate-depth earthquake. Broadband velocity-sensor and acceleration-sensor stations correspond to triangles and squares, respectively. Along-arc stations are denoted with black stars. The low-V_P (<7.9 km/sec) zone according to Papazachos *et al.* (1995), corresponding to the low-Q_S upper mantle wedge (60–90 km), is also depicted by a dashed line.

Data Processing

Broadband velocity-sensor records were corrected for instrument response and were high-pass filtered applying an acausal, second order, Butterworth filter for noise removal. After several tests the corner frequency of the high-pass filter was chosen to have a conservative fixed value of 0.05 Hz, which reflects the high quality of the broadband velocity-sensor data set. The acceleration-sensor records processing included instrument response correction and filtering for removal of environmental and digitizer noise. The filtering procedure followed for ITSAK records was the one applied in Skarlatoudis and Margaris (2006), following the results of Boore (2003, 2005). For acceleration-sensor records for which no pre-event or time mark was available, a simple filtering procedure for noise removal was applied. This procedure was based on three aspects: (1) the visual inspection of the Fourier spectra of both horizontal and the vertical components of the record; (2) the constrain of the velocity time series to oscillate around zero at the end of the record; and (3) the peak values of acceleration, velocity, and displacement to occur approximately at the same time. Most of the acceleration-sensor stations used are installed in soil categories C or D, while all velocity-sensor stations used are installed in soil category B/A, according to the National Earthquake Hazards Reduction Program (NEHRP) (1994) and Uniform Building Code (UBC) (1997) classification. In Table 1 the distribution of acceleration- and velocity-sensor data is shown. The peak ground values (PGA and PGV) were extracted after numerical integration or differentiation of the acceleration and velocity records from acceleration and

Table 1

Site Classification Proposed by NEHRP (1994) for the Recording Stations Used in This Study

Name	Latitude (° N)	Longitude (° E)	Class
1M41	38.447	23.592	B/A
4M71	38.447	23.592	B/A
ALIB	38.388	24.053	C
AMOS	36.796	25.769	B/A
ANDR	37.836	24.948	B/A
ANPA	37.032	25.076	B/A
ANS1	36.472	23.101	B/A
APE	37.069	25.531	B/A
ARG	36.216	28.126	B/A
AT01	38.056	24.378	B/A
AT02	38.047	23.864	B/A
AT03	38.027	23.468	B/A
AT04	37.725	24.050	B/A
ATH	37.972	23.717	B/A
ATHA	38.001	23.774	C
ATHC	37.931	23.698	C
ATLA	38.653	22.999	B/A
BALB	39.640	27.880	B/A
BODT	37.062	27.310	B/A
DAT	36.729	27.578	B/A
DMKA	37.990	23.820	B/A
E031	40.674	23.315	D
EVR	38.917	21.809	B/A
FETY	36.635	29.084	B/A
FRM1	40.655	23.299	D
GVD	34.839	24.087	B/A
HAN1	35.518	24.019	D
HER1	35.318	25.102	C
HER2	35.338	25.136	D
IKAR	37.644	26.305	B/A
IOSI	36.735	25.362	B/A
ISKB	41.066	29.059	B/A
ITM	37.179	21.925	B/A
JAN	39.657	20.851	B/A
KAPA	35.640	27.138	B/A
KARN	35.402	23.917	B/A
KARP	35.547	27.161	B/A
KASO	35.412	26.915	B/A
KEAI	37.623	24.319	B/A
KEK	39.713	19.799	B/A
KERA	37.953	23.607	C
KORA	37.930	22.930	D
KOS1	36.983	27.290	C
KOSI	36.745	26.952	B/A
KRN1	36.802	21.961	C
KYT1	36.150	22.983	B/A
KZN	40.307	21.771	B/A
LAST	35.161	25.479	B/A
LIA	39.898	25.183	B/A
LIT	40.101	22.490	B/A
LKD	38.707	20.651	B/A
LKR.	38.651	22.999	B/A
MEGA	37.427	22.060	D
MYKO	37.482	25.384	B/A
NAX1	37.100	25.367	C
NEO	39.307	23.224	B/A
NPS	35.263	25.613	B/A
NVR	41.350	23.862	B/A
PATB	38.240	21.720	D
PE01	38.017	22.028	B/A

(*continued*)

Table 1 (*Continued*)

Name	Latitude (° N)	Longitude (° E)	Class
PE02	37.896	22.491	B/A
PE04	37.601	22.959	B/A
PE05	37.513	22.455	B/A
PE06	37.179	21.925	B/A
PE07	37.148	22.820	B/A
PE09	36.792	21.888	B/A
PLG	40.374	23.446	B/A
PRK	39.246	26.272	B/A
PRSA	38.020	23.690	C
RDO	41.146	25.538	B/A
RLS	38.058	21.467	B/A
RNTA	37.960	23.680	D
RODN	36.380	28.084	B/A
RODS	36.012	27.820	B/A
S1	39.646	22.409	D
SAMO	37.704	26.838	B/A
SANT	36.371	25.459	B/A
SERI	37.161	24.485	B/A
SIVA	35.018	24.81	B/A
SMG	37.709	26.837	B/A
SOH	40.822	23.354	B/A
STC1	40.664	23.291	B/A
SYRO	37.457	24.927	B/A
THE	40.633	22.966	B/A
THVC	38.320	23.318	C
TILO	36.449	27.354	B/A
TUR1	38.087	26.868	B/A
TUR2	37.642	27.242	B/A
TUR3	37.466	27.538	B/A
TUR4	37.080	27.808	B/A
TUR5	37.030	27.317	B/A
TUR6	37.016	28.426	B/A
TUR7	36.702	27.570	B/A
TUR8	36.827	28.939	B/A
TUR9	36.702	28.089	B/A
VLI	36.720	22.950	B/A
VLS	38.177	20.590	B/A
W021	40.661	23.260	D
W031	40.660	23.251	D
XLCA	38.080	22.630	D
ZKR	35.115	26.217	B/A

broadband velocity sensors correspondingly, for both horizontal components of each record.

Attenuation Properties

Since the first studies of attenuation properties of intermediate-depth earthquakes, it has been noticed that a different attenuation pattern often exists between back-arc and along-arc areas. This phenomenon is also pronounced and well known since the 1970s for the Aegean subduction zone (e.g., Papazachos and Comninakis, 1971). The large number of available data from the Kythera earthquake and their spatial distribution gives the opportunity to look into this pattern in more detail. In Figure 2 the adopted back-arc and along-arc distribution of the recording stations used is presented (along-arc stations are denoted with the black stars). The PGA and PGV values of each record for back-arc and along-arc areas are plotted in Figure 3, where back-arc peak values are denoted with the black circles, while along-arc peak values are denoted with the gray squares. For the PGA values it can be seen that back-arc recordings exhibit a different attenuation trend in comparison with

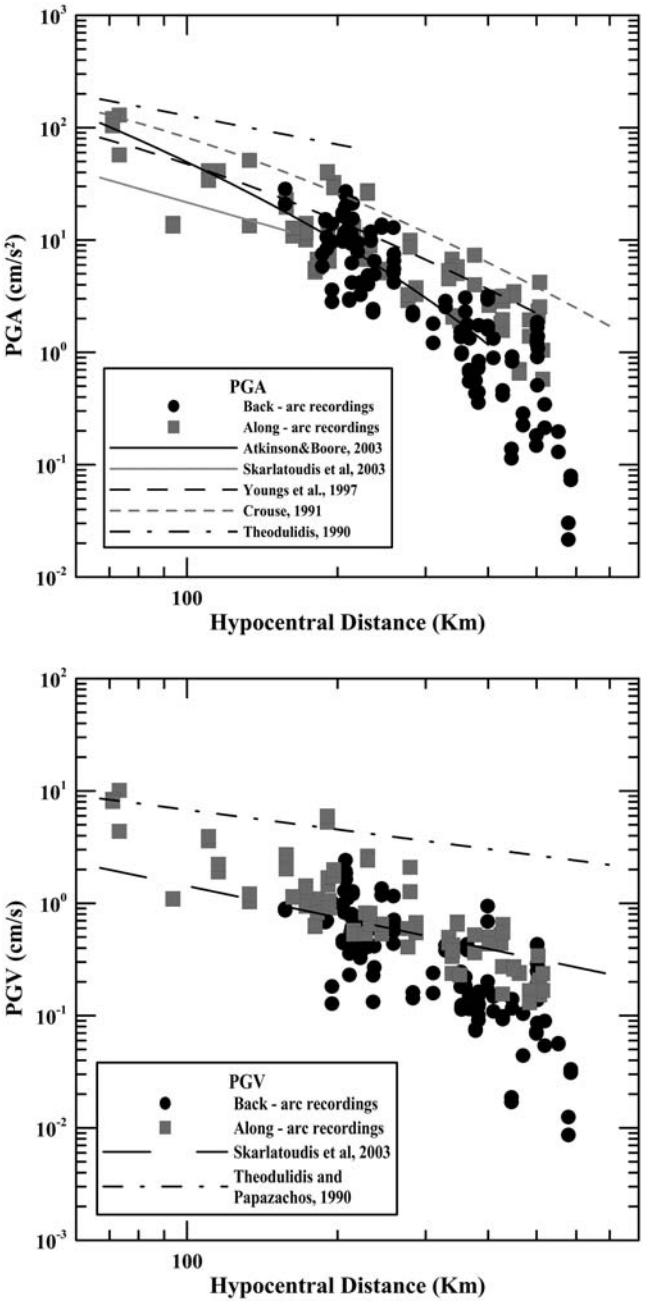

Figure 3. Peak ground values (acceleration and velocity) plotted against hypocentral distance for back-arc and along-arc recordings together with empirical prediction relations for intermediate-depth earthquakes proposed by Theodulidis and Papazachos (1990) (black dashed-dotted line), Crouse (1991) (gray dashed line), Youngs *et al.* (1997) (black dashed line), Atkinson and Boore (2003) (black solid line) and Skarlatoudis *et al.* (2003) for shallow crustal earthquakes (gray solid line) for **M** 6.7 reduced to rock soil conditions.

the along-arc ones, which show a much weaker attenuation with distance. The previous assumption applies also for PGV values, but the difference in the trend is not as prominent, as we gradually move from PGA to PGV.

This difference in the distance decay of the peak values of back-arc recordings (strongest attenuation with distance) in comparison with the along-arc ones is mainly attributed to the low-Q_S (also low-V_S) values of the mantle wedge below the southern Aegean volcanic arc. This low $V_P - V_S$ (and Q_S) layer has been identified by several tomographic studies (Spakman, 1988; Spakman *et al.*, 1993; Papazachos *et al.*, 1995; Papazachos and Nolet, 1997). Because of the subduction of the Mediterranean lithospheric plate, hydrous minerals are dehydrated at the depth of ~80 km. The water released is acting as an accelerator for the partial melting of high-temperature (> 1000°C) materials above the relatively cool subducting slab, forming the high partial-melt mantle wedge, with volcanism representing its surface manifestation. This partial melting can be directly related to the low *P*-and-*S*-wave velocity (low Q_S) zone in the mantle wedge, explaining the back-arc attenuation in the upper mantle above the subducting slab (Papazachos *et al.*, 2000). In Figure 2 the low-V_P ($V_P < 7.9$ km/sec) wave velocity (low Q_S) zone (Papazachos *et al.*, 1995) in the mantle wedge (60–90 km), is depicted by a dashed line verifying the proposed separation of along-arc and back-arc recording stations. It should be pointed out that differences between back-arc and along-arc recordings may also be enhanced due to additional reasons, for instance, refraction of the propagating waves along the high-velocity/low-attenuation channel of the subducting slab (Fukushima, 1997).

Figure 4 schematically describes how this structural pattern affects the *S*- (and also *P*-) wave propagation from intermediate-depth events (like the Kythera event). Direct *S* (and *P*) waves generated at depths > 60 km propagate along the low-temperature/high-*Q* slab and arrive at the outer Hellenic arc, whereas propagation along the back-arc area partly penetrates the low-Q_S mantle wedge beneath the volcanic arc, especially at larger epicentral distances. As a consequence, amplitudes at higher frequencies (affecting mostly PGA values) are significantly reduced, resulting in a stronger attenuation for these stations. This effect is more prominent for deeper events (90–170 km) that generate waves that have a larger ray segment in the low-*Q* mantle wedge, as well as for *S* waves compared to *P* waves, because the mantle wedge partial melt, estimated from petrogenetic results (Zelimer, 1998) and seismological constrains (Karagianni *et al.*, 2005) to locally exceed 15%, affects mostly *S* velocities and Q_S values. On the other hand, for intermediate-depth events with smaller depths (60–90 km), this effect is evident at larger

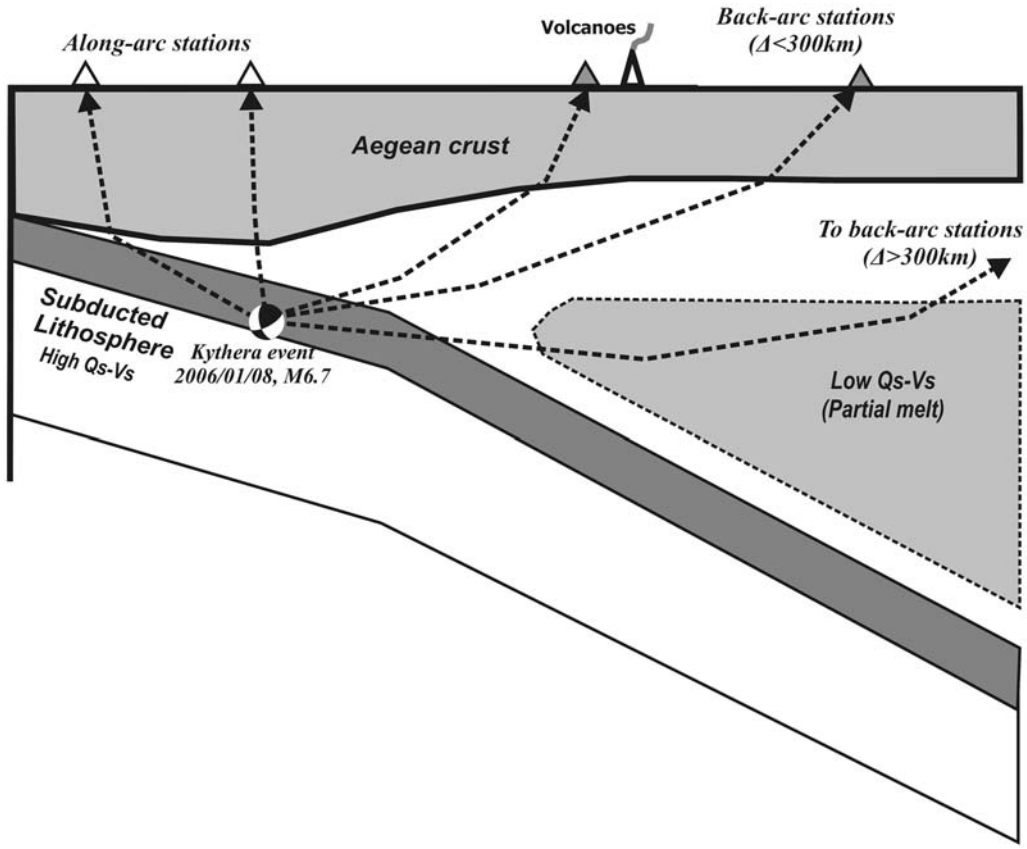

Figure 4. Schematic representation of the wave propagation from the Kythera intermediate-depth event, separating the along-arc and back-arc stations.

epicentral distances (~300 km for the Kythera event, as later shown), because for relatively small epicentral distances, *S* waves are not attenuated by the low-Q region.

The previous assumptions are also in good agreement with another interesting feature derived from Figure 3, namely the reduction of the difference of the decay rate between back-arc and along-arc recordings, as we move from PGA to PGV. This observation can be attributed to the fact that moving from PGA to PGV corresponds to a gradual migration to longer periods, which are less affected by the anelastic attenuation (low-Q_S values) of the mantle wedge. Consequently PGV is expected to be gradually more insensitive to the spatial variation of the anelastic attenuation factor for *S* waves, Q_S.

The previously described features can be also verified by estimating the PGV/PGA ratio for each single station. Traditionally this quantity has been used for site effects assessment (Seed *et al.*, 1976), because rock sites are usually richer in higher frequencies (low PGV/PGA values) while sedimentary sites are usually richer in lower frequencies (high PGV/PGA values). In our case, considering the fact that the vast majority of the recording stations (EGELADOS and broadband velocity-sensor permanent stations) are installed on rock sites, this ratio essentially reflects the different anelastic attenuation between back-arc and along-arc recordings, corresponding to high and low PGV/PGA values, respectively. In Figure 5 (top panels) the PGV/PGA values corrected for distance dependence are plotted against the azimuth with respect to the earthquake epicenter for each recording station. The black solid line represents a running average, while the gray solid line corresponds to a smooth polynomial fit for the computed data. The shaded box shows the azimuths where the ratio exhibits its highest values (approximately from −10° to 90°). The top left-hand panel shows the ratio variation for all back-arc recording stations, while the top right-hand panel shows the ratio for the back-arc recording stations with hypocentral distances greater than 300 km. In the map of Figure 5 (bottom panel) the area for these azimuths (−10° to 90°) and the recording stations with hypocentral distances greater than 300 km are also depicted. It can be easily seen that these azimuths practically correspond to the back-arc area (see also Fig. 2), where we are expecting significant anelastic attenuation effects on higher frequencies, resulting in relatively lower PGA values, that is, high values of the PGV/PGA ratio.

As previously described, the high-frequency attenuation effect observed in back-arc sites is more prominent for intermediate-depth earthquakes. As shown in Figure 5 (top panels) this effect for the Kythera event can be observed only for hypocentral distances greater than 300 km. This distance dependence of the PGV to PGA ratio can be attributed to the relatively shallow depth of the Kythera intermediate-depth event. In the Kythera case seismic waves were propagated for distances less than about 300 km in the crust without being affected by the low-velocity (low Q_S) layer while for greater hypocentral distances seismic waves traveled through the low-velocity (low Q_S) layer exhibiting the higher values of PGV to PGA ratio shown in Figure 5. The previous conclusions are also shown schematically in Figure 4.

Nevertheless, similar anomalous attenuation features have been also observed for shallower earthquakes (e.g., Macias *et al.*, 2008). Moreover in northeast Japan Hashida (1989) reported very low Q-values (about 50) for the first 30 km of continental crust and Singh *et al.* (2006) found similar low-Q attenuation for the Mexican subduction zone. In all studies conducted so far (e.g., Margaris *et al.*, 2002; Skarlatoudis *et al.*, 2003) for the attenuation characteristics of shallow crustal earthquakes in the broader Aegean area, such anomalous behavior has not been identified yet.

Empirical Prediction Relations

The only available empirical prediction relation for intermediate-depth earthquakes applied to the broader Aegean area was derived by Theodulidis and Papazachos (1990) with the use of data from similar seimotectonic environments worldwide. Studies for the derivation of PGA empirical prediction relations for subduction zones have been also conducted by Crouse (1991), Youngs *et al.* (1997), Atkinson and Boore (2003), among others. The comparison of these studies for **M** 6.7 and rock site conditions with the observed data from the 2006 Kythera earthquake is shown in Figure 3. In the same figure, the empirical prediction relation for PGA by Skarlatoudis *et al.* (2003) for shallow earthquakes derived for the broader Aegean area is also shown. The poor agreement of the Skarlatoudis *et al.* (2003) relation with the observed data reflects the totally different properties in wave propagation and attenuation of shallow and intermediate-depth earthquakes in the Aegean area.

The majority of the relations presented in Figure 3 were derived using exclusively acceleration-sensor data. The Atkinson and Boore (2003) (AB2003) relation was derived for interface and in-slab events using acceleration-sensor data and a small number of broadband velocity-sensor recordings from different subducting regions. In Figure 3 a very good agreement of the AB2003 relation with the observed data can be observed, following the strong decay at far-source distances, a feature that all the other relations failed to predict. This issue could be partly attributed to the use of both broadband velocity-sensor and acceleration-sensor data in the relation of AB2003 similar to our data set.

In some cases, the exclusive use of acceleration-sensor data in ground-motion empirical prediction relations can introduce a systematic bias in the derivation of prediction relations. This is mostly due to the fact that recordings at large distances with amplitudes smaller than the trigger level of the acceleration-sensor instruments are not included in the regression analysis because they cannot be recorded. The lack of observations with amplitudes below the triggering level at large distances can result in attenuation results with smaller decay at large distances (Fukushima, 1997). This problem can be overcome with the use of standard broadband

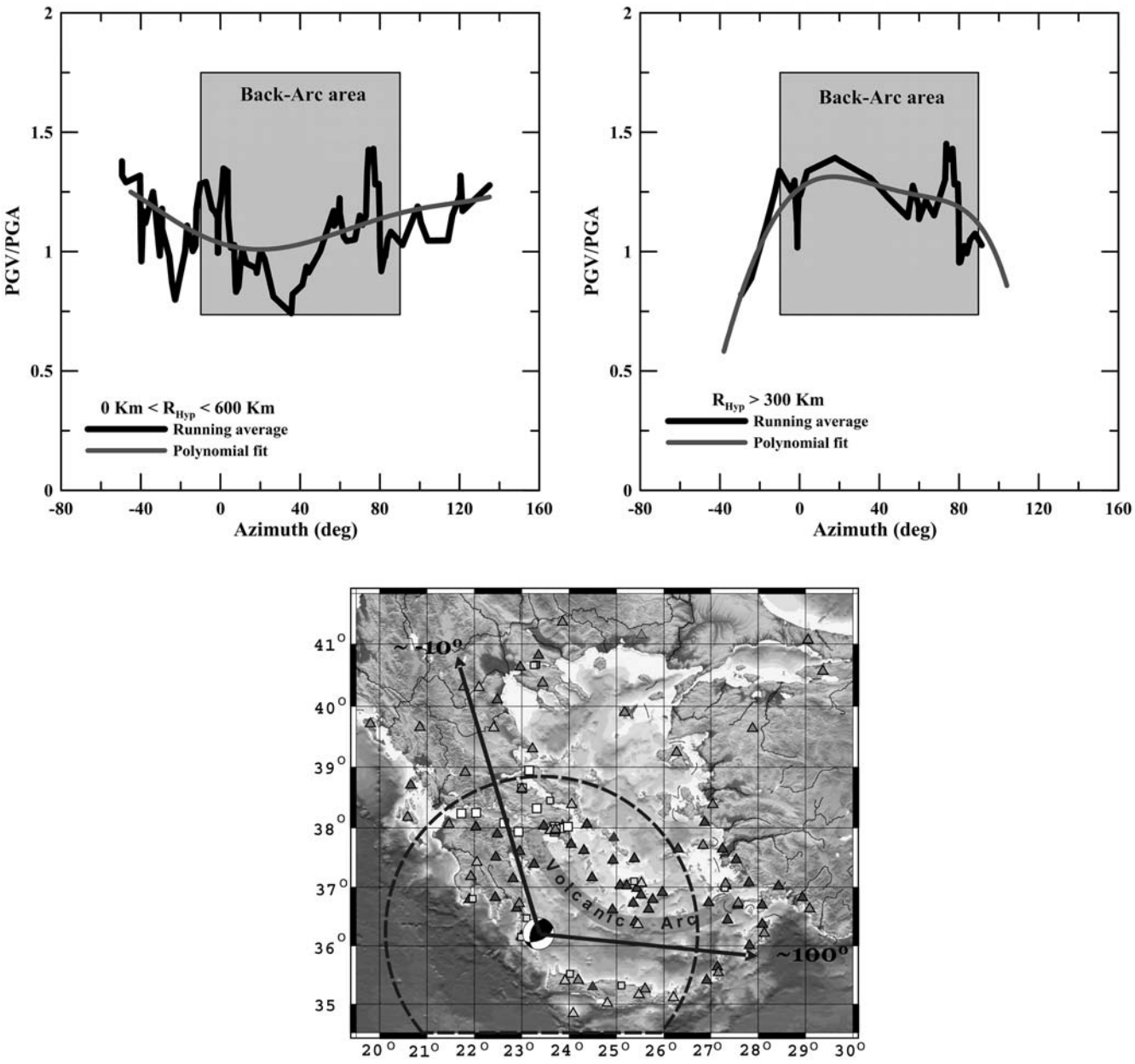

Figure 5. PGV to PGA ratio plotted against azimuth for all recording stations (top left-hand panel) and for recording stations with hypocentral distances greater than 300 km corrected for distance dependence (top right-hand panel). The hatched area shows the azimuths between −10° and 90° (back-arc area). The gray solid line is a polynomial fit to the data, while the black solid line is a running average. The ratio exhibits high values in the hatched area (back-arc area) only for hypocentral distances greater than 300 km. Bottom panel: station separation in along- and back-arc area types, on the basis of PGV/PGA values (azimuths −10°–90°). The dashed circle extends to hypocentral distances up to 300 km.

velocity-sensor instruments, which usually have a much higher sensitivity than acceleration-sensor instruments and can reliably record ground motions at very large distances.

Derivation of Empirical Prediction Relations

For the regression analysis in the present study two functional forms were used:

$$\log Y = c_1 + c_2 \log R + c_3 R + c_{41} S + c_{42} SS \qquad (1a)$$

and

$$\log Y = c_1 + c_2 \log R + c_{31} R_{\text{back}} + c_{32} R_{\text{along}} + c_{41} S + c_{42} SS, \qquad (1b)$$

where Y is PGA (cm/sec^2) and $R = \sqrt{D^2 + h^2}$ with D being the epicentral distance in kilometers and h the hypocentral depth (67 km). S is equal to 1 for NEHRP C soil conditions and 0 otherwise, and SS is equal to 1 for NEHRP D soil con-

Table 2
Regression Coefficients for PGA and PGV, Using Equations (1a) and (1b), for the Kythera Event Data

	c_1	c_2	c_3	c_{31}	c_{32}	c_{41}	c_{42}	σ
PGA (1a)	3.464	−0.821	−0.003	—	—	0.200	0.408	0.31
PGA (1b)	3.396	−0.830	—	−0.0033	−0.0022	0.293	0.461	0.25
PGV (1a)	3.050	−1.287	−0.001	—	—	0.239	0.460	0.27
PGV (1b)	2.988	−1.295	—	−0.0014	−0.0003	0.322	0.508	0.21

ditions and 0 otherwise (NEHRP, 1994; UBC, 1997). In the analysis the geometric mean of the horizontal components was used in order to decrease the inner-station variability of the data. Both equations (1a) and (1b) were used for the regression analysis of the joined data set derived from back-arc and along-arc data. Equation (1b) uses the same geometrical attenuation term (coefficient c_2) for both types of data but accounts for different anelastic attenuation coefficients (coefficients c_{31} and c_{32}) for each one of them. The geometrical attenuation is assumed to be the same (coefficient c_2) for both subdata sets, despite the small difference in the relative position of the recording stations with respect to the subduction zone. This approach may be questioned by the fact that refracted waves may preferentially propagate along the high-Q subducting slab, resulting in higher amplitude recordings at some along-arc stations. However, the detailed analysis of this frequency-dependent phenomenon would require a complete 3D wave propagation analysis, which is out of the scope of this study and has not been used in similar empirical prediction attenuation studies (e.g., Atkinson and Boore, 2003). On the other hand, the anelastic attenuation properties between the two subdata sets should differ due to the different Q_S values in back-arc and along-arc travel paths as previously described in detail in the text. Because no available prediction equations for velocity for intermediate-depth earthquakes are widely used, both equations were also used to derive preliminary coefficients for PGV prediction equations. The regression analysis gave the results shown in Table 2 for the coefficients to be determined.

In Figure 6 a comparison of the observed PGA values and the proposed empirical prediction relations are shown for different data sources (top panel) and for different types of data (bottom panel). In Figure 7a,b empirical prediction relations for PGA (top left-hand panel) and PGV (top right-hand panel) derived in the present study using equations (1a) and (1b) are plotted against the observed values, reduced to rock site conditions ($S = SS = 0$). The corresponding residuals are shown in the bottom panels, plotted against the hypocentral distance together with the ± 1 standard deviation curves (dashed curves) from equation (1b), using black circles for the back-arc data and open circles for the along-arc data, respectively. From the distribution of the resulting residuals it is quite clear that no apparent residual trend can be identified.

A comparison of the PGA relation of the present study with the AB2003 curve exhibits a very good agreement for the distance range for which both are valid. In general, results from the comparison of the PGV relations with the observed data also exhibit a good fit. These results should be considered as preliminary because they are derived from a single earthquake, and the functional form used in the regression

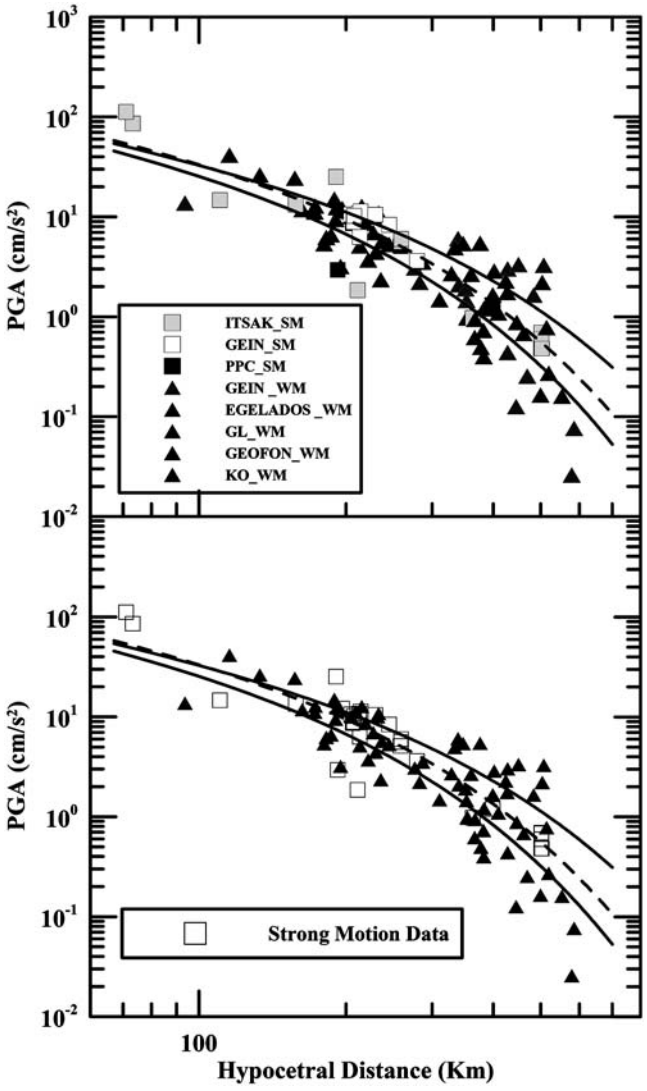

Figure 6. Empirical prediction relations for PGA derived in the present study for equations (1a) (black dashed line) and (1b) (back arc, black solid line; along arc, gray solid line) and rock soil conditions, plotted together with observed data separated by institute (top panel) and by type (bottom panel) reduced to rock soil conditions.

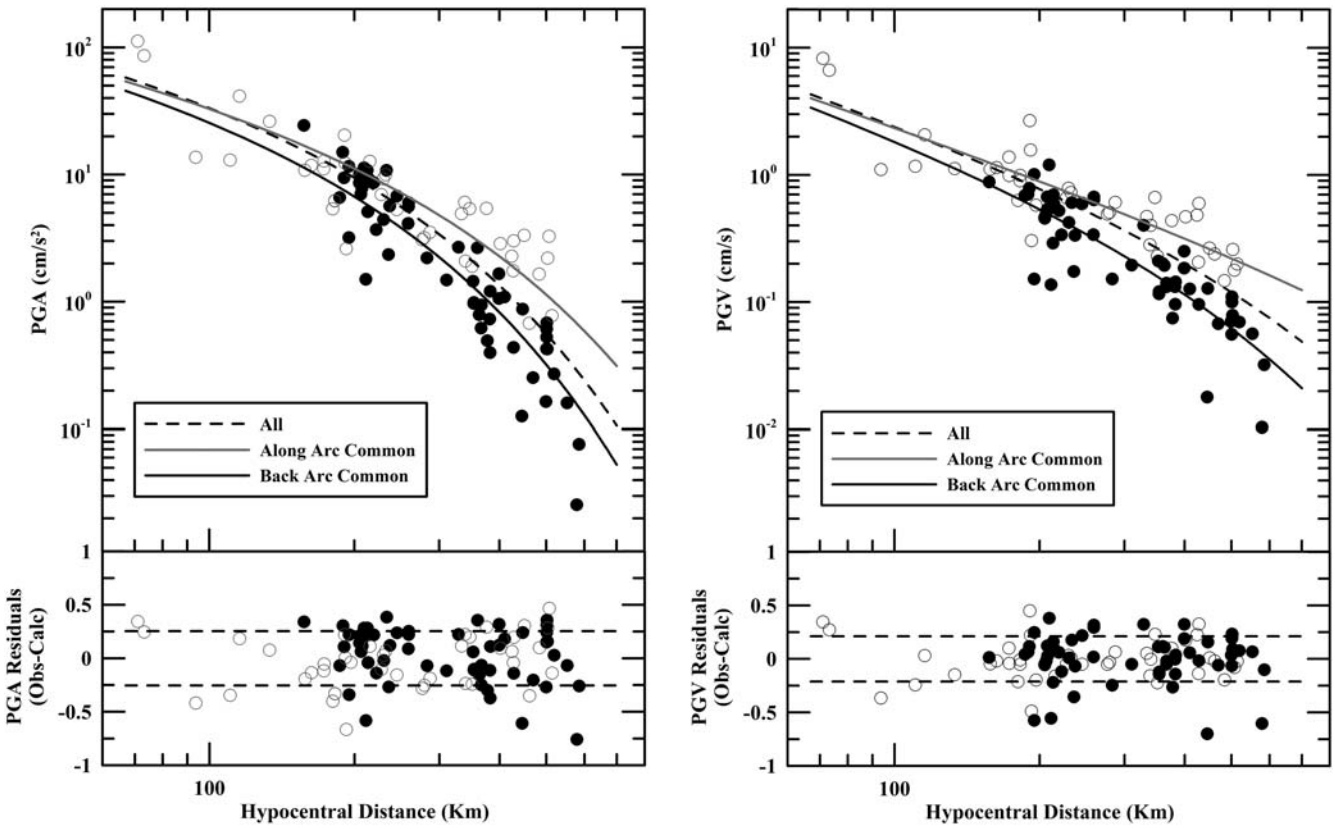

Figure 7. Empirical prediction relations for PGA (top left-hand panel) and PGV (top right-hand panel) derived in the present study using equations (1a) (black dashed line) and (1b) (back arc, black solid line; along-arc, gray solid line) plotted together with the observed values, reduced to rock site conditions. The corresponding residuals are shown in the bottom panels, plotted against hypocentral distance together with the ± 1 standard deviation curves (dashed curves) from equation (1b). Solid and open circles correspond to back-arc data and along-arc data, respectively.

was based on a simplified version of the AB2003 form for PGA. However, the large amount of data used and the good agreement with the AB2003 relation suggest that the proposed relation should be considered as quite representative for intermediate-depth peak ground-motion attenuation for the Aegean subduction zone.

Discussion and Conclusions

All studies conducted for the seismotectonic properties and velocity structure of the southern Aegean subduction zone have pointed out the importance of the low-velocity–low-Q_S layer for the attenuation of the seismic wave propagation from intermediate-depth earthquakes. In the present study the large data set from the 2006 Kythera earthquake allowed us to verify the expected effect of the subduction structure on broadband velocity-sensor and acceleration-sensor records. The combined use of these data revealed a difference in the attenuation pattern between the back-arc and along-arc recordings, with the first exhibiting the strongest anelastic attenuation with distance (linear term in equation 1b), probably due to the low-Q_S mantle wedge of the southern Aegean subduction zone. Moreover, PGV recordings also exhibit a different attenuation in comparison with PGA for back-arc recordings at large epicentral distances where anelastic attenuation plays an important role.

The combined use of strong and broadband velocity-sensor data in the derivation of empirical prediction relations for intermediate-depth earthquakes proved successful because the exclusive use of acceleration-sensor data can, in some cases, introduce significant uncertainties and/or bias. Despite the fact that the inclusion of recordings with somewhat high ground motions at far-source distances due to refraction of the propagating waves along the subducting slab cannot be avoided, it is important to notice that the bias of empirical prediction relations due to the trigger effect (lack of observations with amplitudes below the triggering level) introduced by the acceleration-sensor instruments can be compensated for with the use of higher sensitivity broadband velocity-sensor instruments that reliably record ground motions at very large distances.

Finally, an effort for derivation of new preliminary PGA and PGV empirical prediction relations for intermediate-depth earthquake for the broader Aegean area has been performed. Results from comparison of the PGA relation derived in the present study with the AB2003 relation show that they are in good agreement for the range of distances

that they are both valid. Moreover, PGV preliminary relations exhibit a good fit with the observed data, but additional tests have to be performed to validate its use for practical purposes.

Data and Resources

Velocity-sensor data used in this study were collected using the permanent Greek seismological networks, operated by the National Observatory of Athens and the Aristotle University of Thessaloniki, and are available to the public upon request. The main body of broadband velocity-sensor recordings for this earthquake came from the EGELADOS temporary network and cannot be released to the public. Additional broadband velocity-sensor recordings were used from the Kandilli Observatory and Earthquake Research Institute (KOERI) and GEOFON and are available from the corresponding online databases, http://barbar.koeri.boun.edu.tr/sismo/zKDRS/login.asp (last accessed January 2009) and http://geofon.gfz-potsdam.de/cgi-bin/geofon//request?mode=nform&nettype=perm (last accessed January 2009), respectively.

Acceleration-sensor data used in this study were collected using the acceleration-sensor networks operated by the Institute of Engineering Seismology and Earthquake Engineering (ITSAK), the National Observatory of Athens, the Public Power Corporation (PPC), and the Astronomical Observatory of Larissa. Data from ITSAK and National Observatory of Athens networks are available under request, while data from the other acceleration-sensor networks cannot be released to the public.

Some plots were made using the Generic Mapping Tools version 4.2.1 (Wessel and Smith, 1998; www.soest.hawaii.edu/gmt, last accessed January 2009).

Acknowledgments

We would like to thank G. Atkinson, D. Boore and two anonymous reviewers for their fruitful comments and suggestions, which helped to improve the manuscript. We are also grateful to the Public Power Corporation and the Astronomical Observatory of Larissa for their contribution to the acceleration-sensor data set of this work. This work is partially supported by project 81106#Res.Comm. Univ. of Thessaloniki (funded by the Regional Operational Programme of Crete), the EGELADOS project and the European Community project International Transfer of Seismological Advanced Knowledge and Geophysical Research—ITSAK-GR.

References

Atkinson, G. M., and D. M. Boore (2003). Empirical ground-motion relations for subduction-zone earthquakes and their application to Cascadia and other regions, *Bull. Seismol. Soc. Am.* **93,** 1703–1729.

Benetatos, C., and A. Kiratzi (2006). Source characteristics of the 8 January 2006 (M_w 6.7) intermediate depth Kythera earthquake, in *1st European Conf. on Earthquake Engineering and Seismology*, Geneva, Switzerland, 3–9 September 2006.

Boore, D. M. (2003). Analog-to-digital conversion as a source of drifts in displacements derived from digital recordings of ground acceleration, *Bull. Seismol. Soc. Am.* **93,** 2017–2024.

Boore, D. M. (2005). On pads and filters: processing strong-motion data, *Bull. Seismol. Soc. Am.* **95,** 745–750.

Crouse, C. B. (1991). Ground-motion attenuation equations for earthquakes on the Cascadia subduction zone, *Earthq. Spectra* **7,** 201–236.

Fukushima, Y. (1997). Comment on "Ground motion attenuation relations for subduction zones", *Seism. Res. Lett.* **68,** 947–949.

Hashida, T. (1989). Three-dimensional seismic attenuation structure beneath the Japanese islands and its tectonic and thermal implications, *Tectonophysics* **159,** 163–180.

Karagianni, E. E., C. B. Papazachos, D. G. Panagiotopoulos, P. Suhadolc, A. Vuan, and G. F. Panza (2005). Shear velocity structure in the Aegean area obtained by inversion of Rayleigh waves, *Geophys. J. Int.* **160,** 127–143.

Karakostas, C., T. Makarios, V. Lekidis, T. Salonikios, S. Sous, K. Makra, A. Anastasiadis, N. Klimism, P. Dimitriou, B. Margaris, C. Papaioannou, and N. Theodulidis (2006). The Kythera (Greece) earthquake of January 8, 2006: preliminary report on strong motion data, geotechnical and structural damage, *Earthq. Eng. Res. Inst.*: available at http://www.eeri.org/lfe/pdf/greece_kythira_ITSAK.pdf, 21 pp.

Kiratzi, A., and C. B. Papazachos (1995). Active deformation of the shallow part of the subducting lithospheric slab in the southern Aegean, *J. Geodyn.* **19,** 65–78.

Konstantinou, I. K., I. S. Kalogeras, N. S. Melis, M. C. Kourouzidis, and G. N. Stavrakakis (2006). The 8 January 2006 earthquake (M_w 6.7) offshore Kythira Island, southern Greece: seismological, strong-motion, and macroseismic observations of an intermediate-depth event, *Seism. Res. Lett.* **77,** 544–553.

Macias, M., G. Atkinson, and D. Motazedian (2008). Ground-motion attenuation, source, and site effects for the 26 September 2003 M 8.1 Tokachi-Oki earthquake sequence, *Bull. Seismol. Soc. Am.* **98,** no. 4, 1947–1963.

Margaris, B. N., C. B. Papazachos, Ch. Papaioanou, N. Theodoulidis, I. Kalogeras, and A. A. Skarlatoudis (2002). Empirical attenuation relations for the horizontal strong ground motion parameters of shallow earthquakes in Greece, in *Proc. of the 12th European Conf. on Earthquake Engineering*, London, 9–13 September.

National Earthquake Hazards Reduction Program (NEHRP) (1994). FEMA report 222A: recommended provisions for seismic regulations for new buildings and other structures, Part 1: provisions, Building Seismic Safety Council, Washington D.C., 290 pp.

Papazachos, B. C., and P. E. Comninakis (1971). Geophysical and tectonic features of the Aegean arc, *J. Geoph. Res.* **76,** no. 35, 8517–8533.

Papazachos, C. B., and G. Nolet (1997). *P* and *S* deep velocity structure of the Hellenic area obtained by robust nonlinear inversion of travel times, *J. Geoph. Res.* **102,** 8349–8367.

Papazachos, C. B., P. M. Hatzidimitriou, D. G. Panagiotopoulos, and G. N. Tsokas (1995). Tomography of the crust and upper mantle in southeast Europe, *J. Geophys. Res.* **100,** 12,405–12,422.

Papazachos, B. C., V. G. Karakostas, C. B. Papazachos, and E. M. Scordilis (2000). The geometry of the Wadati-Benioff zone and lithospheric kinematics in the Hellenic arc, *Tectonophysics* **319,** 275–300.

Seed, B., R. Murarka, J. Lysmer, and I. M. Idriss (1976). Relationships of maximum acceleration, maximum velocity, distance from source, and local site conditions for moderately strong earthquakes, *Bull. Seismol. Soc. Am.* **66,** 1323–1342.

Singh, S. K., J. F. Pacheco, D. Garcia, and A. Iglesias (2006). An estimate of shear-wave *Q* of the mantle wedge in Mexico, *Bull. Seismol. Soc. Am.* **96,** no. 1, 176–187.

Skarlatoudis, A. A., and B. N. Margaris (2006). Kythera 2006 Earthquake: data processing of strong motion from various digital sensors, *1st European Conf. on Earthquake Engineering and Seismology*, Geneva, Switzerland, 3–9 September 2006.

Skarlatoudis, A. A., C. B. Papazachos, B. N. Margaris, N. Theodulidis, C. Papaioannou, I. Kalogeras, E. M. Scordilis, and V. Karakostas (2003). Empirical peak ground motion predictive relations for shallow earthquakes in Greece, *Bull. Seismol. Soc. Am.* **93,** 2591–2603.

Spakman, W. (1988). Upper mantle delay time tomography with an application to the collision zone of the Eurasian, African, and Arabian plates, *Ph.D. Thesis*, University of Utrecht, **53,** 200 pp.

Spakman, W., S. Vander Lee, and R. D. Van der Hilst (1993). Travel-time tomography of the European-Mediterranean mantle down to 1400 km, *Phys. Earth Planet. Interiors* **79,** 3–74.

Theodulidis, N., and B. Papazachos (1990). Strong motion from intermediate depth subduction earthquakes and its comparison with that of shallow earthquakes in Greece, in *Proc. of the XXII General Assembly ESC*, Barcelona, 1990, II, 857–864.

Uniform Building Code (UBC) (1997). *Itern. Conf. Building Officials, USA*, Vol. **II**, 489 pp.

Youngs, R. R., S.-J. Chiou, W. J. Silva, and J. R. Humphrey (1997). Strong ground motion attenuation relationships for subduction zone earthquakes, *Seism. Res. Lett.* **68,** 58–73.

Wessel, P., and W. H. F. Smith (1998). New, improved version of the generic mapping tools released, *EOS Trans. AGU* **79,** 579.

Zelimer, G. F. (1998). Petrogenetic processes and their timescales beneath Santorini, Aegean volcanic arc, Greece, *Ph.D Thesis*, Department of Earth Sciences, The Open University Milton Keynes, U.K.

Geophysical Laboratory, School of Geology
University Thessaloniki
PO Box 352-1, GR-54124
Thessaloniki, Greece
askarlat@geo.auth.gr
kpapaza@geo.auth.gr
xrusven@geo.auth.gr
(A.A.S., C.B.P., C.V., D.V.)

Institute of Engineering Seismology and Earthquake Engineering (ITSAK)
Georgikhs Sholis 46, PO Box 53, GR-55102
Thessaloniki, Greece
margaris@itsak.gr
chpapai@itsak.gr
(B.N.M., C.P.)

Institute of Geology, Mineralogy and Geophysics
Ruhr-University Bochum
44780 Bochum, Postfach 10 21 48
44721 Bochum, Germany
bruestle@geophysik.ruhr-uni-bochum.de
meier@geophysik.ruhr-uni-bochum.de
friederich@geophysik.rub.de
(A.B., T.M., W.F.)

Institute of Geodynamics
National Observatory of Athens
PO Box 20048
118 10, Athens, Greece
g.stavr@gein.noa.gr
(G.S.)

Seismology Section
Department of Geophysical Engineering
Istanbul Technical University
Ayazaga Campus
34390-Maslak-Istanbul, Turkey
taymaz@itu.edu.tr
(T.T.)

Seismology Section
Department Physics of the Earth
GeoForschungsZentrum (GFZ)
D-14473, Potsdam, Germany
kind@gfz-potsdam.de
(R.K.)

Department of Mineral Resources Engineering
Technical University of Crete
27 El. Venizelou Street. Chania
Crete, GR-73 133, Greece
vafidis@mred.tuc.gr
(A.V.)

Institute of Geophysics
University of Hamburg
Geomatikum Bundesstrasse 55
D-20146 Hamburg, Germany
torsten.dahm@zmaw.de
(T.D.)

http://www.geophysik.ruhr-uni-bochum.de/research/egelados/
(EGELADOS)

Manuscript received 21 August 2007